ADVANCED FUNCTIONAL MATERIALS
www.afm-journal.de

Three-Dimensional Heteroatom-Doped Carbon Nanofiber Networks Derived from Bacterial Cellulose for Supercapacitors

*Li-Feng Chen, Zhi-Hong Huang, Hai-Wei Liang, Huai-Ling Gao, and Shu-Hong Yu**

Recently, heteroatom-doped three-dimensional (3D) nanostructured carbon materials have attracted immense interest because of their great potential in various applications. Hence, it is highly desirable to exploit a simple, renewable, scalable, multifunctional, and general strategy to engineer 3D heteroatom-doped carbon nanomaterials. Herein, a simple, eco-friendly, general, and effective way to fabricate 3D heteroatom-doped carbon nanofiber networks on a large scale is reported. Using this method, 3D P-doped, N,P-co-doped, and B,P-co-doped carbon nanofiber networks are successfully fabricated by the pyrolysis of bacterial cellulose immersed in H_3PO_4, $NH_4H_2PO_4$, and H_3BO_3/H_3PO_4 aqueous solution, respectively. Moreover, the as-prepared N,P-co-doped carbon nanofibers exhibit good supercapacitive performance.

1. Introduction

New strategies for material fabrication are of fundamental importance in the development of science and technology.[1,2] The engineering of carbon nanomaterials by substituting some atoms with heteroatoms, such as nitrogen (N), phosphorus (P), boron (B), sulphur (S), iodine (I), and so on, is an effective way to tailor their electron-donor properties,[3,4] and consequently tune the electrical and chemical performance of their surface.[5,6] As a result, heteroatom-doped nanostructured carbon materials have been the focus of immense interest because of their great potential in a large variety of applications, including catalysis,[7,8] gas adsorption,[9] biosensing,[10] bioimaging,[11] energy conversion,[12,13] energy storage systems,[7,14–17] and other electronic devices.[18,19] In particular, three-dimensional architectures are recognized to have extensive application potential.

With tremendous interests, worldwide researchers have devoted great efforts on the rational design and fabrication of heteroatom-doped carbon nanomaterials. In the past decades, there has been certain success in developing effective approaches for synthesizing heteroatom-doped carbon nanomaterials.[10,12,16–21] However, despite great progress has been made, the preparation of different heteroatom-doped carbon materials is rarely a general strategy; furthermore, the preparation of these existing heteroatom-doped carbon materials, specifically 3D network monolith, usually involves either complicated and expensive instruments, or harsh, complex, and time-consuming synthesis routes, or hazardous chemicals (e.g., concentrated sulfuric acid), all that have seriously restricted their practical applications. Accordingly, it is highly desirable to exploit a simple, renewable, scalable, but multifunctional and general strategy to effectively engineer 3D heteroatom-doped carbon nanomaterials, which is crucial for widespread implementation and commercialization.

Bacterial cellulose (BC), a bio-product produced from fermentation, has attracted much attention due to its wide availability, low cost, renewability, and porous nature.[6,14,22,23] Herein, we demonstrate a highly efficient, convenient, low-cost, and general strategy to fabricate heteroatom-doped carbon nanomaterials based on the characteristic abundant surface functional groups (hydroxy/carboxylic groups) of BC,[24] in which the BC serves as an excellent platform for introducing different heteroatoms into the framework of carbon nanomaterials. Specifically, P-doped, N,P-co-doped, and B,P-co-doped carbon nanofibers were successfully prepared by impregnating H_3PO_4, $NH_4H_2PO_4$, and H_3BO_3/H_3PO_4 into the BC pellicle, respectively, followed by carbonization in an inert atmosphere at 800 °C. Compared with previous reports, our approach has three significant advantages for constructing 3D macroscopic heteroatom-doped carbon materials, namely, i) the raw materials are abundant and cheap, ii) the preparation process is easy handling, versatile, and general, and iii) the fabrication is generally suitable for an industrial scale-up. To demonstrate the application potential of the as-prepared heteroatom-doped carbon nanomaterials, here we show the utilization of N,P-co-doped carbon nanofibers in electrode materials of supercapacitor devices. The as-constructed supercapacitor exhibits high power density and excellent cycling stability.

L.-F. Chen, Z.-H. Huang, H.-W. Liang, H. L. Gao, Prof. S. H. Yu
Division of Nanomaterials and Chemistry
Hefei National Laboratory for Physical Sciences at Microscale
Collaborative Innovation Center of Suzhou Nano Science and Technology
Department of Chemistry
Department of Materials Science and Engineering
University of Science and Technology of China
Hefei, Anhui 230026, China
E-mail: shyu@ustc.edu.cn

DOI: 10.1002/adfm.201400590

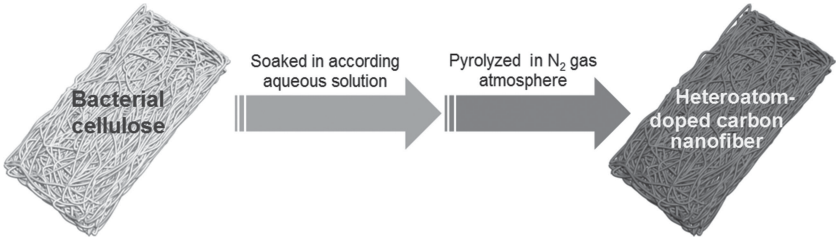

Scheme 1. Schematic representation of the fabrication process of the free-standing heteroatom-doped carbon nanofibers.

2. Results and Discussion

2.1. Synthesis and Identification of Three-Dimensional Heteroatom-Doped Carbon Nanofibers

The general strategy for fabricating free-standing heteroatom-doped carbon nanofibers is illustrated in **Scheme 1**. Three typical heteroatom-doped carbon materials, namely, P-doped, N,P-co-doped, and B,P-co-doped carbon nanofibers, are adopted to verify the feasibility and versatility of our synthesis route. In the fabrication process, the BC was firstly immersed in an aqueous solution of H_3PO_4, $NH_4H_2PO_4$, or H_3BO_3/H_3PO_4 for 10 h at room temperature. Then, the resulting samples were dried followed by an easy thermal annealing in the atmosphere of nitrogen gas. All raw materials and reagents involved in the fabrication are quite low-cost; moreover, the aqueous solution can easily diffuse into the void volume of the macroscopic-scale BC pellicle. Therefore, it is very easy to produce heteroatom-doped carbon nanofibers at industrial scale. Importantly, the amount of heteroatoms doped in the carbon materials could be easily tailored by controlling the mass of the according precursor (CHN elemental analysis of N,P-co-doped carbon nanofiber, Supporting Information, Table S1). Here, to demonstrate the efficiency and adaptability of our proposed approaches, typical N,P-co-doped carbon nanofibers (N,P-CNF) obtained from thermal decomposition of BC previously immersed in 0.1 mol L^{-1} $NH_4H_2PO_4$ are taken as an example.

The original BC pellicle exhibits a water-rich morphology (**Figure 1**a), revealing its strong hydrophilic property, which results from the presence of numerous hydroxyl groups along its network.[23] Further characterization by scanning electron microscopy (SEM) illustrates that the BC consists of coadjacent nanofibrils and cross-linked pores (Supporting Information, Figure S1a). Moreover, we find that the as-prepared material still retains the intrinsic highly porous and ultrafine network nanostructures of original BC pellicles; the carbon nanowires are interconnected with numerous junctions (Figure 1b,c). Transmission electron microscopy (TEM) measurements show that the diameter of these nanofibers is 16–25 nm (Supporting Information, Figure S1b). Such nanofibers with small sizes provide a high surface-to-volume ratio increasing the interfacial area; this unique 3D nanofiber network architecture will enable fast electron and ion transport along all 3D directions within the heteroatom-doped carbon material, rather than normal to the layers.[17,23] High resolution transmission electron microscopy (HRTEM) (Figure 1d) further indicates that these nanofibers in the heteroatom-doped carbon materials mainly consist of randomly orientated graphitic layers, although some turbostratic carbon may exist. Energy filter TEM (EFTEM) mapping images (Figure 1e–i) reveal that heteroatoms are effectively incorporated and homogeneously distributed throughout the pellicles at the nanoscale, meanwhile, demonstrating that heteroatom-doped carbon nanomaterials are successfully manufactured in the easy, low-cost, and scalable process.

Comparing electron energy loss spectroscopy (EELS) taken from as-prepared heteroatom-doped carbon nanofibers and pure carbon nanofibers (pure CNF) pyrolyzed from the original

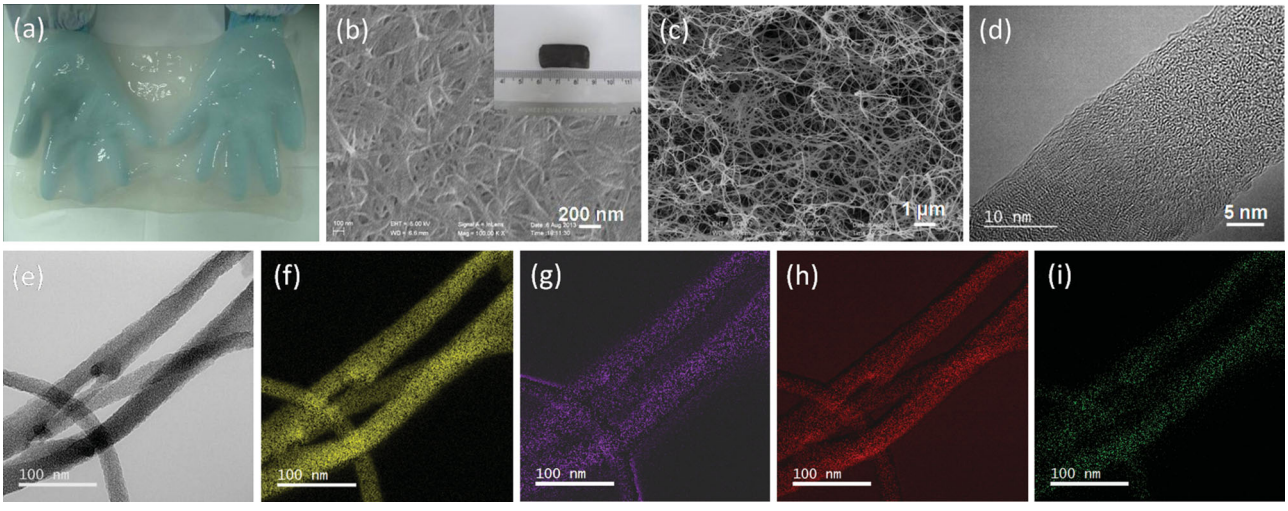

Figure 1. a) Photograph of a BC pellicle. b) SEM image of the N,P-co-doped carbon nanofiber surface (inset: the typical sample, 2.7×1.2 cm^2). c) SEM image of the inner of N,P-co-doped carbon nanofiber (N,P-CNF). d) HRTEM image of the N,P-CNF. e) Typical energy filter TEM (EFTEM) image of N,P-CNF. f-i) Corresponding elemental mapping images of f) C, g) N, h) P, and i) O.

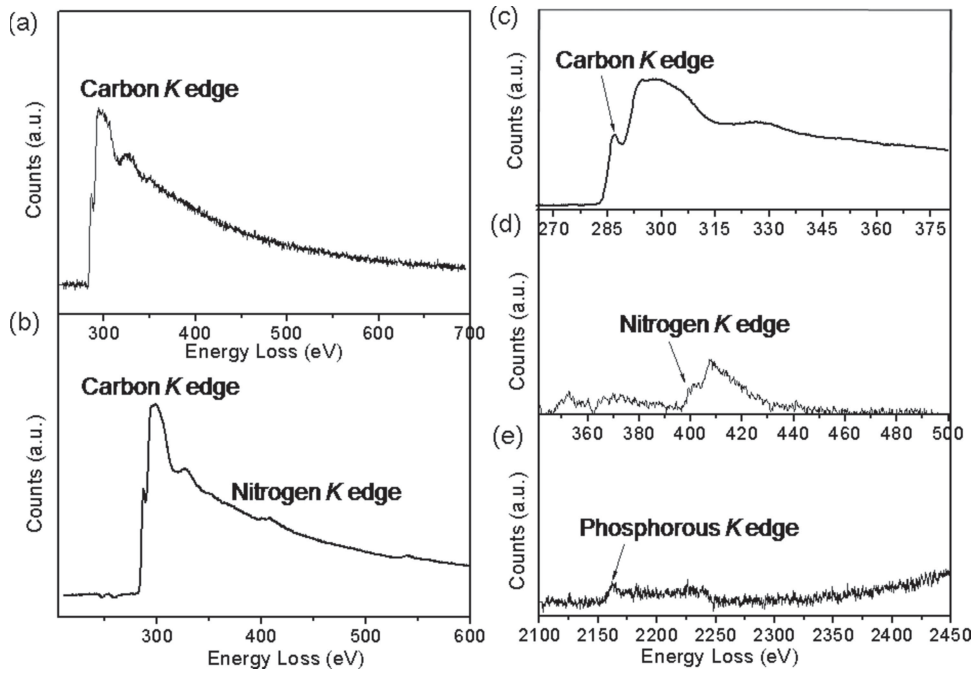

Figure 2. a) Electron energy loss spectroscopy of pure carbon nanofibers (pure CNF). b–e) EELS spectra of N,P-CNF.

bacterial cellulose (**Figure 2**a,b), we observe the simultaneous presence of C, N, and P elements in the N,P-CNF. Moreover, Figure 2c–e also confirm that nitrogen and phosphor are co-doped in the carbon nanofibers.[5,20,25] Afterward, Fourier transform infrared (FTIR) spectra were used to identify functional groups in the samples. In the spectra of N,P-CNF (**Figure 3**a), two peaks appear at 1250 and 1360 cm^{-1} corresponding to the C-N bond[11] and in-plane stretching vibrations within the heterocylic rings of graphite-like structures,[3] respectively, which demonstrates the successful introduction of heteroatoms into the carboatomic ring.

X-ray photoelectron spectra (XPS) further confirm that the heteroatoms are incorporated into the carbon nanofibers. The characteristic peaks in the survey spectra suggest that the as-prepared sample indeed is co-doped with N and P in the carbon framework (Supporting Information, Figure S2). Moreover, the binding environments of both N and P could be elucidated by the high-resolution XPS spectra (Figure 3b,c). The high-resolution spectrum of the N1s peak can be divided into two forms of nitrogen functional groups, namely, pyridinic (N-6, 398.7 ± 0.1 eV) and pyrrolic/pyridine (N-5, 401.09 ± 0.1 eV),[15] indicating that there are two species of nitrogen atoms in the sample (Figure 3b). Meanwhile, the deconvolution of the high-resolution P2p peak spectrum yields two peaks, and the main peak at 133.46 eV (Figure 3c) corresponds to P-C binding.[26] Accordingly, this method is efficient for introducing nitrogen/phosphorus heteroatoms into the carbon frameworks. In addition, the XPS results show that the N,P-CNF is doped with 5.76 atom% of nitrogen and 3.72 atom% of phosphorus; just the high ratio of N-5 and P-C functionalities can provide a large number of active sites to improve its capacitive properties.[27]

The Raman spectra in Figure 3d also confirm the presence of graphitic layers within the heterocyclic carbon nanofibers, where two peaks at 2800 ± 45 and 1575 ± 25 cm^{-1} related to the 2D and G band, respectively, are signatures of graphitic carbon materials.[23] Furthermore, it is found that the G band of the N,P-CNF appears at lower frequency (1575 cm^{-1}) compared to that of pure CNF (1600 cm^{-1}), suggesting the successful introduction of nitrogen/phosphorus into the carbon nanofibers. Such a shift has also been reported in previous research.[28]

Subsequently, the Brunauer-Emmett-Teller (BET) surface area of the N,P-CNF is determined by nitrogen isotherm adsorption-desorption measurement, which shows a specific surface area as high as 289.90 m^2 g^{-1} (**Figure 4**a and Table S2, Supporting Information). In addition, the porous feature with a large number of micropores/mesopores and main pore size of 2.21 nm is further proven by pore-size distribution analysis (Figure 4b and Supporting Information Table S2). The formation of the micropores and mesopores can be ascribed to the gas release of volatile species such as CO, CO_2, acetic acid, etc., during the pyrolysis of the bacterial cellulose/$NH_4H_2PO_4$ precursor.[23]

In addition, we have successfully synthesized other heteroatom-doped carbon nanofibers such as P-doped carbon nanofibers (P-CNF) and B,P-co-doped carbon nanofibers (B,P-CNF) on a large scale using this rational strategy (insets in **Figure 5**a and Figure 5d). From the typical SEM images of P-CNF (Figure 5a-c) and B,P-CNF (Figure 5d–f), it is obvious that 3D porous network structures with ultrafine carbon nanofibers can be fabricated. Furthermore, the corresponding EFTEM mapping images (Figure S3 and S4, Supporting Information), FTIR (Figure S5, Supporting Information),[16] XPS (Figure S6 and S7, Supporting Information),[17,25,26,28] EELS spectra (Figure S8 and S9, Supporting Information),[5,20,25] Raman spectra (Figure S10, Supporting Information),[28] nitrogen adsorption-desorption isotherms (Figure S11a and

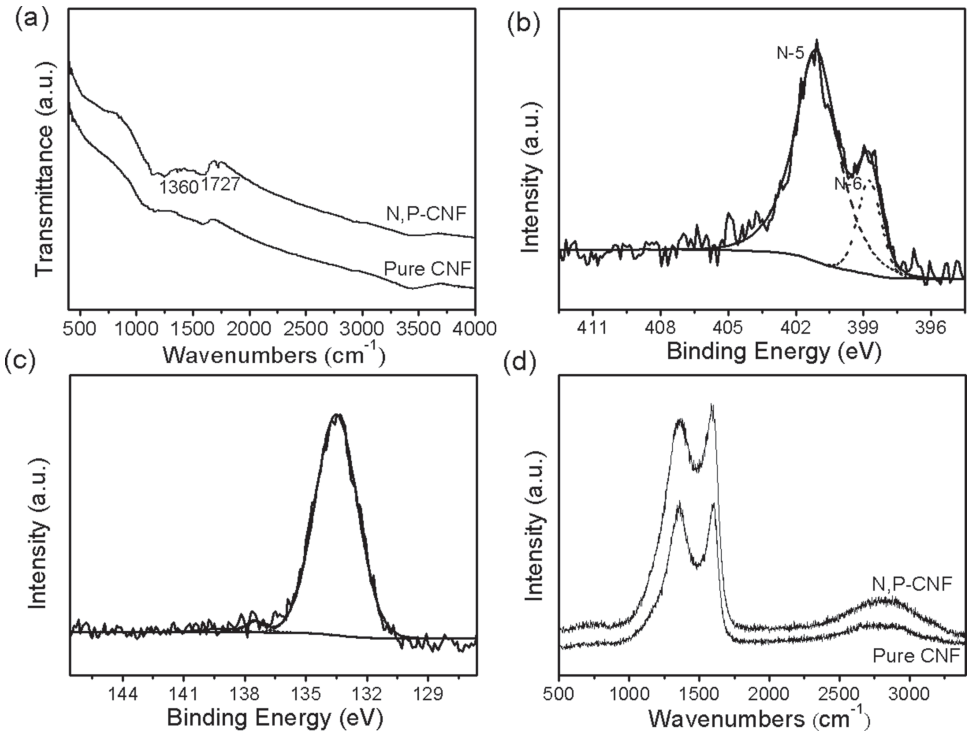

Figure 3. a) FTIR spectra of the pure CNF and N,P-CNF. b,c) High-resolution XPS spectra of deconvoluted N1s and P2p peak of N,P-CNF. d) Raman spectra of the pure CNF and N,P-CNF.

S12a, Supporting Information), and pore size distribution analysis (Figure S11b and S12b, Supporting Information) disclose the highly effective doping of heteroatoms into the carbon nanofibers, indicating the feasibility, effectiveness, and versatility of our method for constructing heteroatom-doped carbon nanofibers with micropores and mesopores. On the basis of the above analysis and the FTIR spectra (Figure S13, Supporting Information), we infer that the synthesis of the heteroatom-doped carbon nanofibers occurs in two steps: firstly, the solvent (H_3PO_4, $NH_4H_2PO_4$, or H_3BO_3/H_3PO_4) is bound with the abundant functional groups (such as OH and C=O) of BC; then, the as-impregnated BC is carbonized to form the heteroatom-doped carbon nanofibers.[3,5,13,29,30]

2.2. Application of N,P-CNF in Supercapacitors

Owing to higher power density than conventional dielectric capacitors and batteries,[31–34] supercapacitors employed in the world market have been growing rapidly, ranging from consumer electronics and hybrid electric vehicles to industrial electric utilities.[35] To further improve the performance of supercapacitors, novel electrode materials with superior properties are highly desirable.[15] It has been widely demonstrated that heteroatom-doped carbon materials exhibit so-called pseudocapacitive performance,[6,7,17,21] which is related to the charge transfer between electrode materials and ions of the electrolyte.[36] Although a large number of carbon materials with monoatomic doping were reported as electrode materials of supercapacitors,[15,17,33] the supercapacitive performance is still required to be further enhanced. Currently, heteroatom-co-doped carbon materials utilized as supercapacitive electrode materials have been researched. However, nitrogen/phosphorus-co-doped carbon materials are rarely reported as electrodes of supercapacitors. Here, we show that as-prepared N,P-CNF are a suitable candidate for supercapacitive electrode materials. In this study, we investigate its capacitive properties in 2.0 M H_2SO_4 aqueous electrolyte with a two-electrode setup reflecting the electrochemical performance of a real capacitor,[36] where the N,P-CNF monoliths were directly fabricated as binder/additive-free working electrodes by cutting the material into small slices of 1.0 cm × 1.0 cm.

Cyclic voltammetry (CV) was measured to probe the electrochemical performance of the N,P-CNF at a potential window of 1.0 V. Interestingly, the CV profiles of the N,P-CNF retain quasi-rectangular shapes as the sweep rate increases from 50 to 700 mV s^{-1} (**Figure 6**a), indicating its good capacitive behavior and high-rate capability. The electrochemical performance of the N,P-CNF was further studied by galvanostatic charge/discharge measurements. We measured the different N,P-CNF-based supercapacitors using a two-electrode system in a 2.0 M H_2SO_4 aqueous electrolyte at a current density of 1.0 A g^{-1} (Figure S14a, Supporting Information) and found that the N,P-CNF//N,P-CNF supercapacitor exhibits a higher specific supercapacitance (C_s) than our other N,P-CNF-based supercapacitors. It is found that increasing the concentration of the $NH_4H_2PO_4$ aqueous solution from 0.02 to 0.05, then to 0.1 mol L^{-1} leads to an increase of C_s (at 1.0 A g^{-1}) from 129.19 to 161.37, then to 204.9 F g^{-1} (Figure S14b, Supporting Information), respectively, owing to the increasing amounts of nitrogen/phosphorus incorporated into the 3D porous carbon network. However, when the concentration of the $NH_4H_2PO_4$

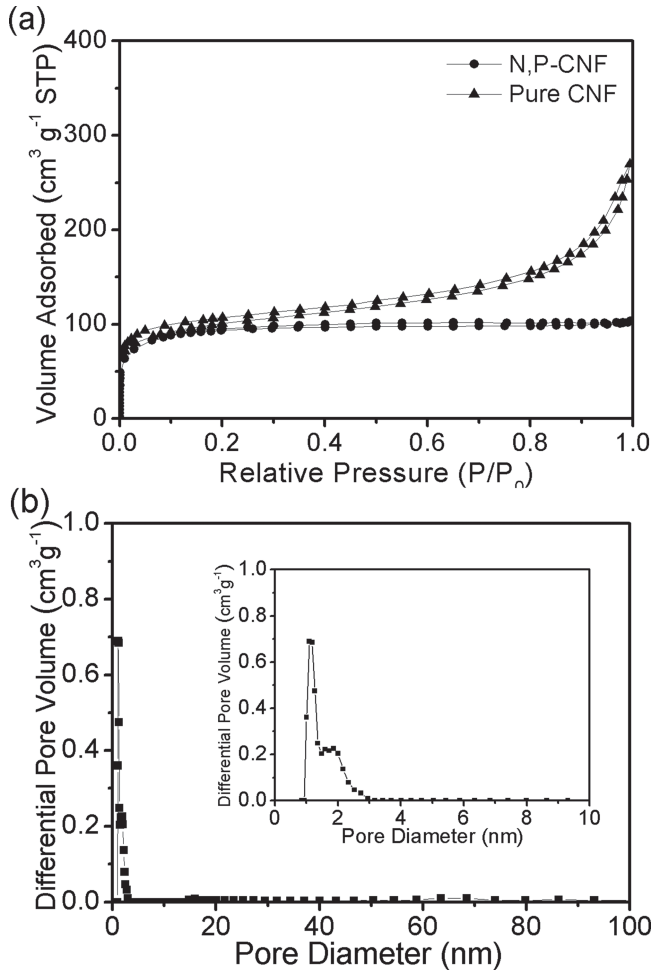

Figure 4. a) Nitrogen adsorption-desorption isotherms of pure CNF and N,P-CNF. b) Pore size distribution of the N,P-CNF (inset: magnified 0–10 nm region).

aqueous solution is increased to 0.2 mol L^{-1}, the as-prepared bacterial cellulose/$NH_4H_2PO_4$ becomes very thin owing to the corrosion of the highly concentrated $NH_4H_2PO_4$ aqueous solution, which results in a lower specific supercapacitance. We also constructed electrochemical capacitors based on pure carbon nanofiber//pure carbon nanofiber (pure CNF//pure CNF), P-carbon nanofiber//P-carbon nanofiber (P-CNF//P-CNF), and B,P-carbon nanofiber//B,P-carbon nanofiber (B,P-CNF//B,P-CNF) with pure-CNF, P-CNF, and B,P-CNF, respectively, using the similar assemble process of the N,P-CNF//N,P-CNF supercapacitor. Their galvanostatic charge-discharge curves at a current density of 1.0 Ag^{-1} (Figure S15, Supporting Information) showed that the N,P-CNF//N,P-CNF supercapacitor exhibits a higher specific supercapacitance than the pure-CNF//pure-CNF, P-CNF//P-CNF, and B,P-CNF//B,P-CNF supercapacitors. In addition, the specific supercapacitance of the as-prepared N,P-CNF is larger than that of the N-doped CNF.[15] The large specific capacitance of the N,P-CNF//N,P-CNF supercapacitor is mainly due to co-doping of nitrogen and phosphorus increasing the capacitance. Therefore, we further investigate the supercapacitor performances of the N,P-CNF//N,P-CNF system.

The charge-discharge curve of the N,P-CNF (Figure 6b) exhibits a nearly triangular shape without obvious *IR* drop at a high current density of 2.0 A g^{-1}, which indicates that the supercapacitor exhibits the high reversibility of a typical capacitor with a rapid *I–V* response and a small equivalent series resistance owing to nitrogen/phosphorus being incorporated into the 3D carbon matrix enhancing the electrical conductivity and wettability between the electrolyte and electrode materials.[15] Meanwhile, the galvanostatic charge/discharge curves collected at various current densities from 1.0 to 50.0 A g^{-1} (Figure 6b) show slightly nonlinear sloping potential profiles, implying that the Faradaic reactions occur on the surface of N,P-CNF, which is consistent with the results of CV.

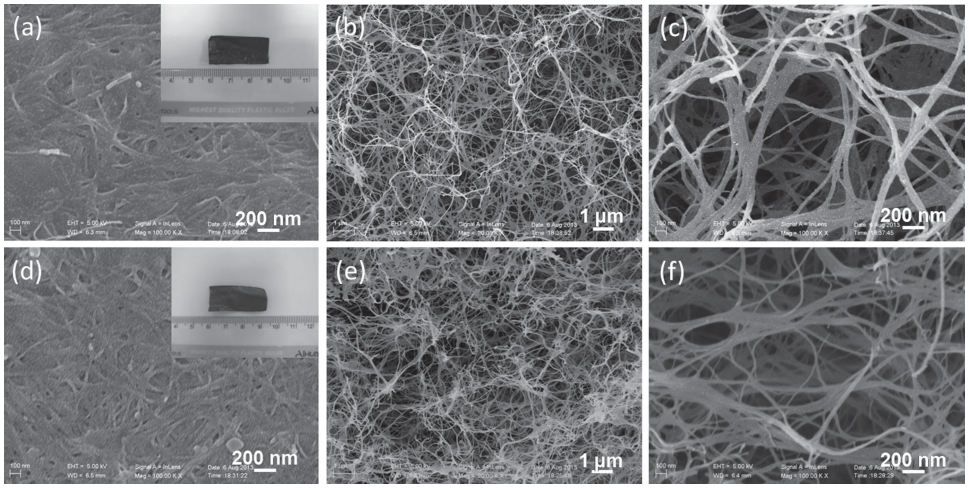

Figure 5. a) SEM image of the P-doped carbon nanofiber (P-CNF) surface (inset: a typical sample, 3.0 × 1.4 cm^2). b) SEM image of the inner of the P-CNF. c) Magnified SEM image of the inner of P-CNF. d) SEM image of the B,P-co-doped carbon nanofiber (B,P-CNF) surface (inset: a typical sample, 3.3 × 1.5 cm^2). e) SEM image of the inner of the B,P-CNF. f) Magnified SEM image of the inner of B,P-CNF.

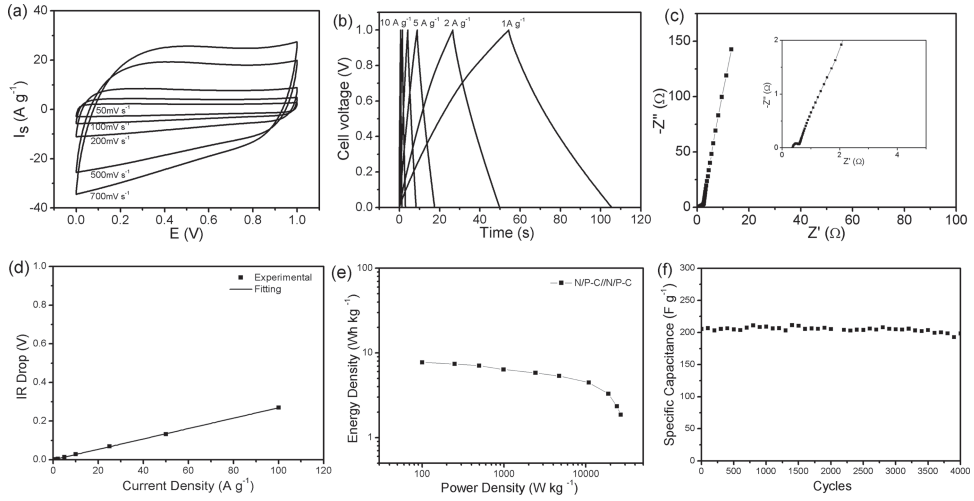

Figure 6. Electrochemical properties of the N,P-CNF//N,P-CNF supercapacitor measured using a two-electrode system in a 2.0 M H_2SO_4 aqueous electrolyte. a) CV curves at different scan rates. b) Galvanostatic charge-discharge curves at different current densities. c) Electrochemical impedance spectra. d) Potential drop (IR_{drop}) at different discharge current densities. e) Ragone plot. f) Cycling performance at a current density of 2.0 A g^{-1}.

Furthermore, electrochemical impedance spectroscopy (EIS) was carried out to investigate the ion-transport behavior and electrical resistance of the supercapacitor using N,P-CNF as electrode materials. Obviously, the Nyquist plot for N,P-CNF//N,P-CNF (Figure 6c) is composed of a semicircle in the high frequency range and a straight sloping line in the low frequency region. Moreover, the diameter of the semicircle revealed that its charge-transfer resistance (R_{ct}) is quite low, 0.367 Ω, which plays an important role in the relatively high specific power density.

After that, specific capacitance values of the electrode materials were calculated via galvanostatic charge/discharge curves. We find that the specific capacitance of N,P-CNF at 1.0 A g^{-1} is about 204.9 F g^{-1}, significantly higher than that of the pure CNF. The enhanced electrochemical performance can be attributed to a pseudocapacitive contribution of the surface functionalities and the electric double-layer capacitance (EDLC). Furthermore, variations of the specific capacitance for N,P-CNF against current density shows that the material possesses a high capacitance retention ratio (Figure S16, Supporting Information), demonstrating fast ion transport within the supercapacitor owing to the abundance of mesopores in the electrode materials and fast diffusion of the electrolyte.[14,33] From the variation of the *IR* drop (IR_{drop}) at different discharge current densities (Figure 6d), we infer that the as-assembled N,P-CNF//N,P-CNF supercapacitor has a small internal resistance (IR_{drop} [V] = 0.0005046 + $\frac{0.002685}{M}$ *I* [A/g]), which favors the high discharge power delivery in practical applications.[14]

To further evaluate the electrochemical performance, a Ragone plot relative to the corresponding energy and power densities is generated (Figure 6e). Clearly, the N,P-CNF//N,P-CNF supercapacitor can deliver a high energy density of 7.76 Wh kg^{-1}, which is much larger than that of the nitrogen-doped graphene hydrogel supercapacitor (4.5 Wh kg^{-1}, 5.0 M KOH) (Table S3, Supporting Information)[37] and the boron/nitrogen co-doped porous carbon supercapacitor (3.8 Wh kg^{-1}, 6.0 M KOH),[30] and is comparable to the boron/nitrogen co-doping graphene supercapacitor (8.7 kW kg^{-1}).[17] When the current density reaches 100 A g^{-1}, the N,P-CNF//N,P-CNF supercapacitor still retains an energy density of 1.86 Wh kg^{-1} with a high power density of 26.61 kW kg^{-1}, which is much larger than that of commercial supercapacitors[38] and other heteroatom-doped carbon based supercapacitors (Table S3, Supporting Information), such as nitrogen-doped graphene sheets (0.558–16.680 kW kg^{-1}, 1.0 M Et_4NBF_4/propylene carbonate),[38] boron-nitrogen co-doped porous carbon (0.201 kW kg^{-1}, 6.0 M KOH),[30] and phosphorus-enriched carbons (3.1 kW kg^{-1}, 1.0 M H_2SO_4).[21] Moreover, the as-fabricated N,P-CNF//N,P-CNF supercapacitor can reach a maximum power density of 186.03 kW kg^{-1}, surpassing most results of heteroatom-doped carbon materials, which demonstrates the effectiveness of the nitrogen/phosphorus-co-doping in improving supercapacitive performance. The high power density is mainly ascribed to the appropriate co-dopant of nitrogen/phosphorus and the 3D porous nanofiber network ensuring good electrical conductivity, meanwhile, avoiding the use of conducting additives and polymer binders, which blocks the pores and increases contact resistance. Good cycling stability is one of the most important characteristics for state-of-the-art supercapacitors. Thus, we tested the cycle performance of the N,P-CNF based supercapacitor. Significantly, the as-prepared supercapacitor exhibits a very stable specific capacitance value within 4000 cycles (Figure 6f), suggesting long-term cyclicity. Hence, based on the aforementioned analysis, we find that the introduction of nitrogen/phosphorus heteroatoms into the carbon nanofiber is an efficient pathway to improve its supercapacitive performance and the as-prepared supercapacitor has the merit of practical applications.

3. Conclusion

In summary, we have presented an effective, general, and rational strategy for the synthesis of heteroatom-doped carbon

fibers derived from bacterial cellulose (BC). The abundant functional groups of BC allow for easy doping with phosphorus, nitrogen/phosphorus, and boron/phosphorus. Moreover, the as-prepared N,P-CNF can be used as electrode materials of high-performance supercapacitors with a maximum power density of 186.03 kW kg^{-1}. This approach not only provides a promising way to design functional carbon based materials with excellent performance for high-power-density supercapacitors, but also serves as a potential candidate for other applications such as in catalysis, gas adsorption, and biosensing.

4. Experimental Section

Chemicals: Purified bacterial cellulose (BC) pellicles with a thickness of 1.0 mm were kindly provided by Ms. C.Y. Zhong (Hainan Yeguo Foods Co., Ltd., China). All other reagents were analytical grade, commercially available from Shanghai Chemical Reagent Co. Ltd, and used as received without further purification.

Preparation of Heteroatom-Doped Carbon Nanofibers: Briefly, the as-received gel-like white purified BC pellicles were firstly neutralized with deionized water (DIW) and then cut into rectangular slices (4.0 cm × 2.0 cm) with a sharp blade; subsequently, four BC slices were immersed in 100 mL of 0.01 mol L^{-1} H_3PO_4, 0.1 mol L^{-1} $NH_4H_2PO_4$, and 0.005 mol L^{-1} H_3BO_3/H_3PO_4 aqueous solution, respectively, under agitation for 10 h at room temperature, and next frozen in liquid nitrogen (−196 °C). The slices were subsequently freeze-dried in a bulk tray dryer (Labconco Corporation, USA) at a sublimating temperature of −50 °C and a pressure of 0.035 mbar for evaporating the solvent. Finally, the as-obtained BC was pyrolyzed in a nitrogen atmosphere at 2.0 °C min^{-1} to 520 °C for 1.0 h and then at 5.0 °C min^{-1} to 800 °C for 1.0 h to form the black product. 1.0 g BC can yield approximately 0.4 g of heteroatom-doped carbon nanofibers. In the preparation process of B,P-co-doped carbon nanofibers (B,P-CNF), the as-pyrolyzed sample was washed in 50–60 °C DIW and subsequently cooled to the room temperature.

In order to control the doping content of nitrogen and phosphorus in the N,P-CNF (N,P-CNF), the molarity of the $NH_4H_2PO_4$ aqueous solution used in the experiment was adjusted. Here, N,P-co-doped carbon nanofiber-1 (N,P-CNF-1), N,P-carbon nanofiber-2 (N,P-CNF-2), N,P-carbon nanofiber (N,P-CNF), N,P-carbon nanofiber-3 (N,P-CNF-3) were prepared with a $NH_4H_2PO_4$ aqueous solution molarity of 0.02 mol L^{-1}, 0.05 mol L^{-1}, 0.1 mol L^{-1}, 0.2 mol L^{-1}, respectively.

Preparation of Pure Carbon Nanofibers: The as-received gel-like white purified BC pellicles were firstly neutralized with deionized water (DIW) and cut into rectangular slices with a sharp blade. Some slices were frozen in liquid nitrogen (−196 °C) and subsequently freeze-dried in a bulk tray dryer (Labconco Corporation, USA) at a sublimating temperature of −48 °C and a pressure of 0.04 mbar. The obtained dry BC was then pyrolyzed in a nitrogen atmosphere at 2.0 °C min^{-1} to 520 °C for 1.0 h and then at 5.0 °C min^{-1} to 800 °C for 1.0 h.

Characterization: SEM images were performed on a Zeiss Supra 40 field-emission scanning electron microanalyzer at an acceleration voltage of 5 kV. Energy filter TEM mapping images and electron energy loss spectroscopy data were obtained on a JEM-ARM 200F Atomic Resolution Analytical Microscope. Raman scattering spectra were taken on a Renishaw System 2000 spectrometer using the 514.5 nm line of Ar^+ for excitation. FTIR measurements were conducted on a Bruker Vector-22 FTIR spectrometer at 4000–400 cm^{-1}. XPS spectra were collected on an ESCALab MKII X-ray photoelectron spectrometer using a Mg Kα radiation exciting source (1253.6 eV). N_2 sorption analysis was carried out on an ASAP 2020 accelerated surface area and porosimetry instrument (Micromeritics), equipped with an automated surface area, at 77 K using Barrett–Emmett–Teller (BET) calculations for the surface area. The pore size distribution (PSD) plot was produced with the adsorption branch of the isotherm based on the Barrett-Joyner-Halenda (BJH) model. The CHN analysis was carried out using an Elementarvario EL cube.

Electrochemical Measurement: All electrochemical measurements were carried out by a two-electrode system at room temperature. Herein, the two-electrode configuration consists of two slices of the free-standing electrode materials with the same size (about 1.0 cm by 1.0 cm), the filter paper (pore size of 225 nm) as separator, and a pair of Pt foils as the current collectors. Then, the supercapacitor assemblies were wrapped with parafilm. Before the construction of assemblies, the electrode materials were soaked in an electrolyte of 2.0 M H_2SO_4 aqueous electrolyte for 6.0 h. CV curves and galvanostatic charge/discharge measurements were recorded at the potential range of 0 to 1.0 V. Electrochemical impedance spectroscopy was tested in the frequency range of 10 mHz–100 kHz. All electrochemical experiments were carried out with a CHI 760D electrochemical workstation at room temperature.

Supporting Information

Supporting Information is available from the Wiley Online Library or from the author.

Acknowledgements

L.-F.C. and Z.-H.H. contributed equally to this work. This work was supported by the Ministry of Science and Technology of China (Grants 2012BAD32B05–4, 2010CB934700, 2013CB933900, 2014CB931800), the National Natural Science Foundation of China (Grants 91022032, 91227103, 21061160492, J1030412), the Chinese Academy of Sciences (Grant KJZD-EW-M01–1), Hainan Province Science and Technology Department (CXY20130046), and the China Postdoctoral Science Foundation (Grant 2014M550346) for financial support. The authors thank Ms C. Y. Zhong for kindly providing purified bacterial cellulose pellicles.

Received: February 20, 2014
Revised: March 29, 2014
Published online: May 30, 2014

[1] X. Wang, J. Zhuang, Q. Peng, Y. D. Li, *Nature* **2005**, *437*, 121.
[2] S. Iijima, *Nature* **1991**, *354*, 56.
[3] Y. Zheng, Y. Jiao, L. Ge, M. Jaroniec, S. Z. Qiao, *Angew. Chem. Int. Ed.* **2013**, *52*, 3110.
[4] D. Jana, C. L. Sun, L. C. Chen, K. H. Chen, *Prog. Mater. Sci.* **2013**, *58*, 565.
[5] L. Song, Z. Liu, A. L. M. Reddy, N. T. Narayanan, J. Taha-Tijerina, J. Peng, G. H. Gao, J. Lou, R. Vajtai, P. M. Ajayan, *Adv. Mater.* **2012**, *24*, 4878.
[6] L. F. Chen, Z. H. Huang, H. W. Liang, W. T. Yao, Z. Y. Yu, S. H. Yu, *Energy Environ. Sci.* **2013**, *6*, 3331.
[7] M. J. Zhong, E. K. Kim, J. P. McGann, S. E. Chun, J. F. Whitacre, M. Jaroniec, K. Matyjaszewski, T. Kowalewski, *J. Am. Chem. Soc.* **2012**, *134*, 14846.
[8] S. B. Yang, L. J. Zhi, K. Tang, X. L. Feng, J. Maier, K. Müllen, *Adv. Funct. Mater.* **2012**, *22*, 3634.
[9] Y. D. Xia, R. Mokaya, G. S. Walker, Y. Q. Zhu, *Adv. Energy Mater.* **2011**, *1*, 678.
[10] Y. Wang, Y. Y. Shao, D. W. Matson, J. H. Li, Y. H. Lin, *ACS Nano* **2010**, *4*, 1790.
[11] Y. Q. Dong, H. C. Pang, H. B. Yang, C. X. Guo, J. W. Shao, Y. W. Chi, C. M. Li, T. Yu, *Angew. Chem. Int. Ed.* **2013**, *52*, 7800.
[12] L. Qie, W. M. Chen, Z. H. Wang, Q. G. Shao, X. Li, L. X. Yuan, X. L. Hu, W. X. Zhang, Y. H. Huang, *Adv. Mater.* **2012**, *24*, 2047.

[13] J. P. Paraknowitsch, A. Thomas, *Energy Environ. Sci.* **2013**, *6*, 2839.
[14] L. F. Chen, Z. H. Huang, H. W. Liang, Q. F. Guan, S. H. Yu, *Adv. Mater.* **2013**, *25*, 4746.
[15] L. F. Chen, X. D. Zhang, H. W. Liang, M. G. Kong, Q. F. Guan, P. Chen, Z. Y. Wu, S. H. Yu, *ACS Nano* **2012**, *6*, 7092.
[16] J. Liang, Y. Jiao, M. Jaroniec, S. Z. Qiao, *Angew. Chem. Int. Ed.* **2012**, *51*, 11496.
[17] Z. S. Wu, A. Winter, L. Chen, Y. Sun, A. Turchanin, X. L. Feng, K. Mullen, *Adv. Mater.* **2012**, *24*, 5130.
[18] X. L. Li, H. L. Wang, J. T. Robinson, H. Sanchez, G. Diankov, H. J. Dai, *J. Am. Chem. Soc.* **2009**, *131*, 15939.
[19] Y. Z. Xue, B. Wu, L. Jiang, Y. L. Guo, L. P. Huang, J. Y. Chen, J. H. Tan, D. C. Geng, B. R. Luo, W. P. Hu, G. Yu, Y. Q. Liu, *J. Am. Chem. Soc.* **2012**, *134*, 11060.
[20] O. Stephan, P. M. Ajayan, C. Colliex, P. Redlich, J. M. Lambert, P. Bernier, P. Lefin, *Science* **1994**, *266*, 1683.
[21] D. Hulicova-Jurcakova, A. M. Puziy, O. I. Poddubnaya, F. Suárez-García, J. M. D. Tascón, G. Q. Lu, *J. Am. Chem. Soc.* **2009**, *131*, 5026.
[22] R. T. Olsson, M. A. S. A. Samir, G. Salazar-Alvarez, L. Belova, V. Strom, L. A. Berglund, O. Ikkala, J. Nogues, U. W. Gedde, *Nat. Nanotechnol.* **2010**, *5*, 584.
[23] B. Wang, X. L. Li, B. Luo, J. X. Yang, X. J. Wang, Q. Song, S. Y. Chen, L. J. Zhi, *Small* **2013**, *9*, 2399.
[24] M. Koyama, W. Helbert, T. Imai, J. Sugiyama, B. Henrissat, *Proc. Natl. Acad. Sci. USA* **1997**, *94*, 9091.
[25] X. C. Zhao, Q. Zhang, B. S. Zhang, C. M. Chen, A. Q. Wang, T. Zhang, D. S. Su, *J. Mater. Chem.* **2012**, *22*, 4963.
[26] J. P. Paraknowitsch, Y. Zhang, B. Wienert, A. Thomas, *Chem. Commun.* **2013**, *49*, 1208.
[27] F. Su, C. K. Poh, J. S. Chen, G. W. Xu, D. Wang, Q. Li, J. Y. Lin, X. W. Lou, *Energy Environ. Sci.* **2011**, *4*, 717.
[28] L. S. Panchalkarla, A. Govindaraj, C. N. R. Rao, *ACS Nano* **2007**, *1*, 494.
[29] D. W. Wang, F. Li, Z. G. Chen, G. Q. Lu, H. M. Cheng, *Chem. Mater.* **2008**, *20*, 7195.
[30] G. Hong Liang, G. Qiu Ming, *J. Power Sources* **2009**, *186*, 551.
[31] Y. P. Zhai, Y. Q. Dou, D. Y. Zhao, P. F. Fulvio, R. T. Mayes, S. Dai, *Adv. Mater.* **2011**, *23*, 4828.
[32] C. Liu, F. Li, L. P. Ma, H. M. Cheng, *Adv. Mater.* **2010**, *22*, E28.
[33] L. Hao, X. L. Li, L. J. Zhi, *Adv. Mater.* **2013**, *25*, 3899.
[34] J. Jiang, Y. Y. Li, J. P. Liu, X. T. Huang, C. Z. Yuan, X. W. Lou, *Adv. Mater.* **2012**, *24*, 5166.
[35] T. Chen, L. M. Dai, *Mater. Today* **2013**, *16*, 272.
[36] D. Hulicova-Jurcakova, M. Kodama, S. Shiraishi, H. Hatori, Z. H. Zhu, G. Q. Lu, *Adv. Funct. Mater.* **2009**, *19*, 1800.
[37] P. Chen, J. J. Yang, S. S. Li, Z. Wang, T. Y. Xiao, Y. H. Qian, S. H. Yu, *Nano Energy* **2013**, *2*, 249.
[38] Y. C. Qiu, X. F. Zhang, S. H. Yang, *Phys. Chem. Chem. Phys.* **2011**, *13*, 12554.